FORCE AND MOMENT ROTORDYNAMIC COEFFICIENTS FOR PUMP-IMPELLER SHROUD SURFACES

Dara W. Childs
Texas A&M University
College Station, Texas 77843

Governing equations of motion are derived for a bulk-flow model of the leakage path between an impeller shroud and a pump housing. The governing equations consist of a path-momentum, a circumferential - momentum, and a continuity equation. The fluid annulus between the impeller shroud and pump housing is assumed to be circumferentially symmetric when the impeller is centered; i.e., the clearance can vary along the pump axis but does not vary in the circumferential direction.

A perturbation expansion of the governing equations in the eccentricity ratio yields a set of zeroth and first-order governing equations. The zeroth-order equations define the leakage rate and the circumferential and path velocity distributions and pressure distributions for a centered impeller position. The first-order equations define the perturbations in the velocity and pressure distributions due to either a radial-displacement perturbation or a tilt perturbation of the impeller. Integration of the perturbed pressure and shear-stress distribution acting on the rotor yields the reaction forces and moments acting on the impeller face.

Introduction

Figure 1 illustrates an impeller stage of a multi-stage centrifugal pump. Leakage along the front side of the impeller, from impeller discharge to inlet, is restricted by a wear-ring seal, while leakage along the back side is restricted by either an interstage seal or a balance-discharge seal. Lomakin [1] originally recognized the major influence that seals have on the rotordynamic response of centrifugal pumps. Recent analysis and test results are provided by references [2-4].

More recently, various investigators have considered the forces developed by flow through the impeller and its interaction with either a volute or a vaned diffuser. Cal Tech researchers [5] have presented measured force coefficients for an impeller precessing in a volute. Ohashi and Shoji [6] also provide measured force coefficients for an impeller whirling in vaneless and vaned diffusers. More recently, Bolleter et al. [7] from Sulzer Brothers, Ltd. have also presented test results for an impeller in a vaned diffuser. The Cal Tech and Sulzer

test programs use conventional impellers in their test programs, but use a radial face seal to minimize or eliminate the forces which would normally be developed by the wear-ring seals. The face seals employed by these investigators sharply reduce the leakage flow down the front face of the impeller. The impeller tested by Ohashi et al. has flat, parallel, front and back shrouds. Test results from all these investigators suggest that impellers create relatively benign forces from a rotordynamic viewpoint. Ohashi concludes that impeller forces would damp forward whirling motion in most operating conditions. The Cal Tech and Sulzer researchers conclude that impellers would provide positive damping unless a rotor's running speed exceeded its critical speed by an approximate factor of 2.5. Hence impellers are predicted to yield smaller destabilizing forces than bearings or long seals which are predicted to yield destabilizing forces when the running speed exceeds twice the critical speed.

There is some contrary evidence from operating pump experience with respect to impeller forces. Specifically, Massey [8] cites experience with an 11-stage pump which was unstable and whirled at 80% of running speed; i.e., the pump was unstable when its running speed was only 1.25 times the critical speed. The HPOTP (High Pressure Oxygen Turbopump) of the SSME also whirled at 80% of running speed [9]. This evidence suggests that some unaccounted-for destabilizing force is present in pumps. The present analysis is aimed at investigating the forces and moments developed by impeller-shroud forces.

A bulk-flow analysis is employed similar to that of Childs and Kim [3]. However the analysis is extended to account for the changing geometry of impeller surface. In addition, the shear stress contribution to the reaction forces is accounted for, and the reaction-moment coefficients are calculated using the approach of reference [10]. Specifically, the following general model is used to define the reaction forces and moments which arise for small motion of a pump impeller about its centered position.

$$-\begin{Bmatrix} F_X \\ F_Y \\ M_Y \\ M_X \end{Bmatrix} = \begin{bmatrix} K & k & k_{\varepsilon\alpha} & -k_{\varepsilon\alpha} \\ -k & K & -k_{\varepsilon\alpha} & -K_{\varepsilon\alpha} \\ K_{\alpha\varepsilon} & k_{\alpha\varepsilon} & K_{\alpha} & -k_{\alpha} \\ k_{\alpha\varepsilon} & -K_{\alpha\varepsilon} & K_{\alpha} & K_{\alpha} \end{bmatrix} \begin{Bmatrix} X \\ Y \\ \alpha_Y \\ \alpha_X \end{Bmatrix} + \begin{bmatrix} C & c & C & -c_{\varepsilon\alpha} \\ -c & C & -c_{\varepsilon\alpha} & -C_{\varepsilon\alpha} \\ C_{\alpha\varepsilon} & c_{\alpha\varepsilon} & C_{\alpha} & -_{\alpha} \\ c_{\alpha\varepsilon} & -C_{\alpha\varepsilon} & c_{\alpha} & C_{\alpha} \end{bmatrix} \begin{Bmatrix} \dot{X} \\ \dot{Y} \\ \dot{\alpha}_Y \\ \dot{\alpha}_X \end{Bmatrix}$$

$$+ \begin{bmatrix} M & 0 & M_{\varepsilon\alpha} & 0 \\ 0 & M & 0 & -M_{\varepsilon\alpha} \\ M_{\alpha\varepsilon} & 0 & M_{\alpha} & 0 \\ 0 & -M_{\alpha\varepsilon} & 0 & M_{\alpha} \end{bmatrix} \begin{Bmatrix} \ddot{X} \\ \ddot{Y} \\ \ddot{\alpha}_Y \\ \ddot{\alpha}_X \end{Bmatrix} \qquad (1)$$

where (F_X, F_Y), (X, Y) define the components of the impeller reaction forces and relative displacements, and (M_Y, M_X), (α_Y, α_X) define the components of the reaction moments and rotation (small-angles) vectors.

Geometry and Kinematics

Figure 1 illustrates the annular leakage paths along the front and back sides of a typical shrouded impeller of a multistage centrifugal pump. The present discussion concentrates on the flow and pressure fields within the forward annulus; however, the analysis also applies to the rear annulus. As illustrated in figure 2, the outer surface of the impeller is a surface of revolution formed by rotating the curve $R = R(Z)$ about the Z axis. A point on the surface may be located by the coordinates Z, R(Z), θ. The length along the curve R(Z) from the initial point R_i, Z_i to an arbitrary point R, Z is denoted by S and defined by

$$S = \int_{Z_i}^{Z} \sqrt{1 + \left(\frac{dR}{dZ}\right)^2}\, du = \int_{R_i}^{R} \sqrt{1 + \left(\frac{dZ}{dR}\right)^2}\, du \qquad (2)$$

In the equations which follow, the path coordinate S and angular coordinate θ are used as independent spatial variables. The coordinates Z,R defining the impeller surface are be expressed as parametric functions of S, i.e., Z(S), R(S).

Trigonometric functions of the angle γ, illustrated in figure 3, are defined as follows

$$\tan\gamma = -\frac{dR}{dZ}$$

$$\cos\gamma = \frac{dZ}{dS}, \quad \sin\gamma = -\frac{dR}{dS} \qquad (3)$$

The clearance between the impeller and the housing is denoted as $H(S,\theta,t)$, with the time dependency introduced by impeller motion. In the centered position, the clearance function depends only on S and is denoted by $H_o(S)$. Displacement of the impeller in the X and Y directions obviously causes a change in the clearance function. The clearance function is also changed by pitching or yawing of the impeller as defined by rotations α_X, α_Y about the X and Y axes, respectively. For small displacements and rotations of the impeller the clearance function can be stated

$$H(S,\theta,t) = H_o(S) - [(X + \alpha_Y Z)\cos\gamma - \alpha_Y R\sin\gamma]\cos\theta$$
$$- [(Y - \alpha_X Z)\cos\gamma + \alpha_X R\sin\gamma]\sin\theta \qquad (4)$$

Observe in this equation that H_o, R, Z, $\cos\gamma$ and $\sin\gamma$ are solely functions of S, while X, Y, α_X, α_Y are functions only of t.

Governing Equations

Returning to figure 2, the path coordinate S and circumferential coordinate Rθ are used to locate a fluid differential element of thickness H(S,θ,t) illustrated in figure 4. From the geometry of figure 4, the continuity equation can be stated

$$\frac{\partial H}{\partial t} + \frac{\partial}{\partial S}(U_s H) + \frac{1}{R}\frac{\partial}{\partial \theta}(U_\theta H) + \left(\frac{H}{R}\right)\frac{\partial R}{\partial S} U_s = 0$$

where U_s and U_θ are the path and circumferential bulk-velocity components, respectively.

Figure 5 illustrates the pressure and shear-stress components acting on the differential fluid element. The first subscripts (s,θ) in the shear-stress definitions (τ_{ss}, τ_{sr}), ($\tau_{\theta s}$, $\tau_{\theta r}$) denote path and θ directions, respectively; the second subscripts (s, r) denote stator and rotor surfaces, respectively. The path momentum equation can be stated

$$-H\frac{\partial P}{\partial S} = -\rho H \frac{U_\theta^2}{R}\frac{dR}{dS} + \tau_{ss} + \tau_{sr}$$

$$+ \rho H \left(\frac{\partial U_s}{\partial t} + \frac{\partial U_s}{\partial \theta}\frac{U_\theta}{R} + \frac{\partial U_s}{\partial S} U_s\right)$$

The circumferential-momentum equation can be stated

$$-\frac{H}{R}\frac{\partial P}{\partial \theta} = \tau_{\theta s} + \tau_{\theta r} + \rho H \left(\frac{\partial U_\theta}{\partial t} + \frac{\partial U_\theta}{\partial \theta}\frac{U_\theta}{R} + \frac{\partial U_\theta}{\partial S} U_s + \frac{U_\theta U_s}{R}\frac{\partial R}{\partial S}\right)$$

Following Hirs' approach [11], the wall shear-stress definitions in these equations can be stated

$$\tau_{ss} = \frac{ns}{2}\rho U_s^2 R_a^{ms}\left[1 + (U_\theta/U_s)^2\right]^{\frac{ms+1}{2}} \qquad (5)$$

$$\tau_{sr} = \frac{nr}{2}\rho U_s^2 R_a^{mr}\left\{1 + \left[(U_\theta - R\omega)/U_s\right]^2\right\}^{\frac{mr+1}{2}}$$

$$\tau_{\theta s} = \frac{ns}{2}\rho U_s U_\theta R_a^{ms}\left[1 + (U_\theta/U_s)^2\right]^{\frac{ms+1}{2}}$$

$$\tau_{\theta r} = \frac{nr}{2}\rho U_s (U_\theta - R\omega) R_a^{mr}\left\{1 + \left[(U_\theta - R\omega)/U_s\right]^2\right\}^{\frac{mr+1}{2}}$$

where

$$R_a = 2H\, U_s / \nu \tag{6}$$

The empirical coefficients (ns, ms), (nr, mr) account for different surface roughnesses on the stator and rotor, respectively.

Impeller-Annulus Geometry

For this analysis, the assumption is made that the impeller is nominally centered in its housing. Hence, in the centered position, the clearance function $H_o(s)$ is only a function of the path coordinate S and does not depend on the azimuthal coordinate $R\theta$. The inlet-clearance function $H_o(0)$, the inlet path velocity $U_s(0)$, and the inlet radius R(0) are denoted, respectively, by C_i, V_i, and R_i. In terms of these variables, leakage volumetric flowrate is defined by

$$\dot{Q} = 2\pi R_i C_i V_i \tag{7}$$

The length of the leakage path along the impeller face is defined by

$$L_s = \int_{Z_i}^{Z_i+L} \sqrt{1+\left(\frac{dR}{dZ}\right)^2}\, dZ \tag{8}$$

Nondimensionalization and Perturbation Analysis

The governing equations define the bulk-flow velocity components (U_s, U_θ) and the pressure P as a function of the coordinates ($R\theta$, S) and time, t. They are conveniently nondimensionalized by introducing the following variables

$$u_s = U_s/V_i,\ u_\theta = U_\theta/R_i\omega,\ p = P/\rho V_i^2$$

$$h = H/C_i,\ s = S/L_s,\ r = R/R_i \tag{9}$$

$$\tau = \omega t,\ b = V_i/R_i\,\omega,\ T = L_s/V_i$$

The objective of the present analysis is to examine the changes in (u_s, u_θ, p) due to changes in the clearance function $h(\theta, s, t)$ caused by small motion of the impeller within its housing. To this end, the governing equations are expanded in the perturbation variables

$$\begin{aligned} u_s &= u_{so} + \varepsilon u_{s1},\ h = h_o + \varepsilon h_1 \\ u_\theta &= u_{\theta o} + \varepsilon u_{\theta 1},\ p = p_o + \varepsilon p_1 \end{aligned} \tag{10}$$

were $\varepsilon = e/C_i$ is the eccentricity ratio. The following equations result:

Zeroth-Order Equations

(a) Path-Momentum Equation

$$\frac{dp_o}{ds} + u_{so}\frac{du_{so}}{ds} - \frac{1}{r}\left(\frac{dr}{ds}\right)(u_{\theta o}/b)^2 + \left(\frac{\sigma_s+\sigma_r}{2}\right)u_{so}^2 = 0 \tag{11a}$$

(b) Circumferential-Momentum Equation

$$2\frac{du_{\theta o}}{ds} + 2\frac{u_{\theta o}}{r}\frac{dr}{ds} + [\sigma_r(u_{\theta o} - r) + \sigma_s u_{\theta o}] = 0 \qquad (11b)$$

(c) Continuity Equation

$$r\, h_o\, u_{so} = 1 \qquad (11c)$$

observe that the continuity equation follows directly from Eq. (7)

First-Order Equations

(a) Path-Momentum Equation

$$\frac{\partial p_1}{\partial s} = h_1 A_{1s} - u_{\theta 1} A_{2s} - u_{s1} A_{3s} \qquad (12a)$$
$$- \left[\omega T \frac{\partial u_{s1}}{\partial \tau} + \omega T \frac{u_{\theta o}}{r}\frac{\partial u_{s1}}{\partial \theta} + u_{so}\frac{\partial u_{s1}}{\partial s}\right]$$

(b) Circumferential-Momentum Equation

$$b\,\frac{L_s}{Ri}\frac{1}{r}\frac{\partial p_1}{\partial \theta} = h_1 A_{1\theta} - u_{\theta 1} A_{2\theta} - u_{s1} A_{3\theta} \qquad (12b)$$
$$- \left[\omega T \frac{\partial u_{\theta 1}}{\partial \tau} + \omega T \frac{u_{\theta o}}{r}\frac{\partial u_{\theta 1}}{\partial \theta} + u_{so}\frac{\partial u_{\theta 1}}{\partial s}\right]$$

(c) Continuity Equation

$$\frac{\partial u_{s1}}{\partial s} + \frac{\omega T}{r}\frac{\partial u_{\theta 1}}{\partial \theta} + u_{s1}\left(-\frac{1}{r}\frac{dr}{ds} + \frac{1}{h_o}\frac{dh_o}{ds}\right) =$$
$$- \frac{h_1 u_{so}}{h_o^2}\cdot\frac{dh_o}{ds} - \frac{1}{h_o}\left(u_{so}\frac{\partial h_1}{ds} + \omega T \frac{u_{\theta o}}{r}\frac{\partial h_1}{\partial \theta} + \omega T \frac{\partial h_1}{\partial \tau}\right) \qquad (12c)$$

Most of the parameters of these equations are defined in Appendix A. The quantities σ_s and σ_r are defined by

$$\sigma_s = (L_s/H_o)\,\lambda_s\ ,\ \sigma_r = (L_s/H_o)\lambda_r \qquad (13)$$

where λ_s and λ_r are dimensionless stator and rotor friction factors defined by

$$\lambda_s = ns\, R_{ao}^{ms}\left[1 + (u_{\theta o}/bu_{so})^2\right]^{\frac{ms+1}{2}}$$

$$\lambda_r = nr\, R_{ao}^{mr} \left\{1 + [(u_{\theta o}-r)/bu_{so}]^2\right\}^{\frac{mr+1}{2}}$$

Zeroth-Order-Equation Solutions

The zeroth-order Eqs. (11) define the pressure and velocity distributions for a centered impeller position. For a known volumetric flowrate, the continuity equation completely defines u_{so}. The continuity equations can be used to solve for u_{so} to obtain

$$\frac{du_{so}}{ds} = -u_{so}\left(\frac{1}{h_o}\frac{dh_o}{ds} + \frac{1}{r}\frac{dr}{ds}\right)$$

substituting into Eq. (11a) yields

$$\frac{dp_o}{ds} - \frac{1}{r}\left(\frac{dr}{ds}\right)\frac{u_{\theta o}^2}{b^2} + \left[\left(\frac{\sigma_r+\sigma_s}{2}\right) - \frac{1}{h_o}\frac{dh_o}{ds} - \frac{1}{r}\frac{dr}{ds}\right] u_{so}^2 = 0$$

$$\frac{du_{\theta o}}{ds} + \frac{u_{\theta o}}{r}\frac{dr}{ds} + [\sigma_r(u_{\theta o}-r) + \sigma_s u_{\theta o}]/2 = 0 \qquad (14)$$

Those equations are coupled and nonlinear and must be solved iteratively. The initial condition for $u_{\theta o}(0)$ is obtained from the exit flow condition of the impeller. The inlet and discharge pressure of the impeller are known and serve, respectively, as the exit (P_e) and supply (P_s) pressures for the leakage flow along the impeller face. The inlet conditions for p_o is obtained from the inlet relationship

$$P_s - P_o(0, \theta, t) = \rho(1+\xi) U_{so}^2(0, \theta, t)/2 \qquad (15)$$

From this relationship, the zeroth-order pressure relationship is

$$p_o(0) = P_s/\rho V_i^2 - (1+\xi) u_{so}^2(0)/2 \qquad (16)$$

The impeller exit may also include a restriction yielding a relationship of the form

$$P(L_s,\theta,t) - P_e = \frac{\rho}{2} C_{de} U_s^2 (L_s,\theta,t) \qquad (17)$$

The solution to the zeroth-order Eqs. (14) must be developed iteratively since all of the coefficients depend on the local path velocity U_{so}. In this study, the equations are solved by the following iterative steps:

(a) Guess or estimate V_i which then defines $u_{so}(s)$.
(b) Calculate $p_o(0)$ from Eq. (16), and use a specified $u_{\theta o}(0)$ as initial conditions to numerically integrate Eqs. (14) out to s = 1, i.e., the annulus exit.

(c) Based on the difference between a calculated exit pressure and the prescribed exit pressure, calculate a revised V_i and repeat the cycle until convergence is achieved.

First-order Equations Solutions

The first-order Eqs. (12) define the first-order perturbations $u_{s1}(s,\theta,\tau)$, $u_{\theta 1}(s,\theta,\tau)$, and $p_1(s,\theta,\tau)$ resulting from the perturbed clearance function h_1. From Eqs. (4) and (9), h_1 can be stated

$$\begin{aligned} \varepsilon h_1 &= \left\{ -\left[x+\alpha_Y \left(\frac{L}{Ci}\right) z \right] \cos\gamma + \alpha_Y \left(\frac{Ri}{Ci}\right) r\sin\gamma \right\} \cos\theta \\ &+ \left\{ -\left[y-\alpha_X \left(\frac{L}{Ci}\right) z \right] \cos\gamma - \alpha_X \left(\frac{Ri}{Ci}\right) r\sin\gamma \right\} \sin\theta \\ &= h_{1c}(s,\tau)\cos\theta + h_{1s}(s,\tau)\sin\theta \end{aligned} \tag{18}$$

The theta dependency of the dependent variables is eliminated by assuming the following, comparable solution format

$$\begin{aligned} u_{s1} &= u_{s1c}\cos\theta + u_{s1s}\sin\theta \\ u_{\theta 1} &= u_{\theta 1c}\cos\theta + u_{\theta 1s}\sin\theta \\ p_1 &= p_{1c}\cos\theta + p_{1s}\sin\theta \end{aligned}$$

Substituting into Eqs. (12) and equating like coefficients of $\cos\theta$ and $\sin\theta$ yields six equations in the independent variables s,τ. By introducing the complex variables

$$\begin{aligned} \underline{u}_{s1} &= u_{s1c} + j\, u_{s1s} \quad , \quad \underline{u}_{\theta 1} = u_{\theta 1c} + j\, u_{\theta 1s} \\ \underline{p}_1 &= p_{1c} + jp_{1s} \quad , \quad \underline{h}_1 = h_{1c} + j\, h_{1s} \end{aligned} \tag{19}$$

these real equations are reduced to the following three complex equations in s and τ.

$$\begin{aligned} \frac{\partial \underline{p}_1}{\partial s} &= \underline{h}_1 A_{1s} - \underline{u}_{\theta 1} A_{2s} - \underline{u}_{s1} A_{3s} \\ &- \left[\omega T \frac{\partial \underline{u}_{s1}}{\partial \tau} - j\,\omega T \frac{u_{\theta o}}{r} \underline{u}_{s1} + u_{so} \frac{\partial \underline{u}_{s1}}{\partial s} \right] \end{aligned} \tag{20a}$$

$$\begin{aligned} -j\,\frac{b}{r}\left(\frac{L_s}{R_i}\right) \underline{p}_1 &= \underline{h}_1 A_{1\theta} - \underline{u}_{\theta 1} A_{2\theta} - \underline{u}_{s1} A_{3\theta} \\ &- \left[\omega T \frac{\partial \underline{u}_{\theta 1}}{\partial \tau} - j\,\omega T \frac{u_{\theta o}}{r} \underline{u}_{\theta 1} + u_{so} \frac{\partial \underline{u}_{\theta 1}}{\partial s} \right] \end{aligned} \tag{20b}$$

$$\frac{\partial \underline{u}_{s1}}{\partial s} - j\frac{\omega T}{r}\underline{u}_{\theta 1} + \underline{u}_{s1}\left(-\frac{1}{r}\frac{dr}{ds} + \frac{1}{h_o}\frac{dh_o}{ds}\right) =$$

$$\underline{h}_1\left[\frac{u_{so}}{h_o^2}\frac{dho}{ds} + j\frac{\omega T}{h_o}\frac{u_{\theta o}}{r}\right] - \frac{u_{so}}{h_o}\frac{\partial \underline{h}_1}{\partial s} - \frac{\omega T}{h_o}\frac{\partial \underline{h}_1}{\partial \tau} \qquad (20c)$$

From Eqs. (3) and (17), $\underline{h}_1$ can be stated

$$\varepsilon \underline{h}_1 = -q\left(\frac{L}{L_s}\right)\frac{dz}{ds} - \alpha G_o \qquad (21)$$

where

$$G_o = \left(\frac{L^2}{C_i L_s}\right) z\frac{dz}{ds} + \left(\frac{R_i^2}{C_i L_s}\right) r\frac{dr}{ds} \qquad (22)$$

$$q = x+jy \quad , \quad \alpha = \alpha_Y - j\alpha_X$$

From Eq. (21), the following additional result is obtained

$$\varepsilon\frac{\partial \underline{h}_1}{\partial s} = -q\left(\frac{L}{L_s}\right)\frac{d^2z}{ds^2} - \alpha F_1 \qquad (23)$$

where

$$F_1 = \left(\frac{L^2}{C_i L_s}\right)\left[\left(\frac{dz}{ds}\right)^2 + z\frac{d^2z}{ds^2}\right] + \left(\frac{R_i^2}{C_i L_s}\right)\left[\left(\frac{dr}{ds}\right)^2 + r\frac{d^2r}{ds^2}\right] \qquad (24)$$

The time dependency of Eqs. (20) is eliminated by assuming harmonic seal motion of the form

$$q = q_o e^{jf\tau} \qquad \alpha = \alpha_o e^{jf\tau} \qquad h_1 = h_{1o} e^{jf\tau} \qquad (25)$$

$$f = \Omega/\omega$$

where Ω is the seal whirl frequency and q_o and α_o are real constants. The associated harmonic solution can then be stated

$$\underline{u}_{s1} = \overline{u}_{s1} e^{jf\tau} \qquad \underline{u}_{\theta 1} = \overline{u}_{\theta 1} e^{jf\tau}$$
$$\underline{p}_1 = \overline{p}_1 e^{jf\tau} \qquad (26)$$

Substitution from Eqs. (25) and (26) into the governing complex partial differential equations yields the following three complex ordinary equations in s

$$\frac{d}{ds}\begin{Bmatrix}\bar{u}_{s1}\\ \bar{u}_{\theta 1}\\ p_1\end{Bmatrix} + [A]\begin{Bmatrix}\bar{u}_{s1}\\ \bar{u}_{\theta 1}\\ p_1\end{Bmatrix} = \left(\frac{q_o}{\varepsilon}\right)\begin{Bmatrix}g_1\\ g_2\\ g_3\end{Bmatrix} + \left(\frac{\alpha_o}{\varepsilon}\right)\begin{Bmatrix}g_4\\ g_5\\ g_6\end{Bmatrix} \tag{27}$$

where

(28)

$$[A] = \begin{bmatrix} \left(-\frac{1}{r}\frac{dr}{ds} + \frac{1}{h_o}\frac{dh_o}{ds}\right) & -j\frac{\omega T}{r} & 0 \\ A_{3\theta}/u_{so} & (A_{2\theta} + j\Gamma T)/u_{so} & -j\frac{b}{ru_{so}}\left(\frac{L_s}{R_1}\right) \\ A_{3s} - u_{so}\left(-\frac{1}{r}\frac{dr}{ds} + \frac{1}{h_o}\frac{dh_o}{ds}\right) + j\Gamma T & A_{2s} + j\omega T u_{so} & 0 \end{bmatrix}$$

$$\begin{Bmatrix}g_1\\ g_2\\ g_3\end{Bmatrix} = \left(\frac{L}{L_s}\right)\begin{Bmatrix} F_2 + j\frac{\Gamma T}{ho}\frac{dz}{ds} \\ -\left(\frac{A_{1\theta}}{u_{so}}\right)\frac{dz}{ds} \\ -A_{1s}\frac{dz}{ds} - u_{so}F_2 - ju_{so}\frac{\Gamma T}{h_o}\frac{dz}{ds}\end{Bmatrix} \tag{29}$$

$$\begin{Bmatrix}g_4\\ g_5\\ g_6\end{Bmatrix} = \begin{Bmatrix} F_3 + jG_o\,\Gamma T/h_o \\ -A_{1\theta}G_o/u_{so} \\ -G_oA_{1s} - u_{so}F_3 - jG_ou_{so}\,\Gamma T/h_o\end{Bmatrix} \tag{30}$$

and

$$\Gamma = \omega\,(f - u_{\theta o}/r)$$

$$F_2 = \frac{u_{so}}{ho}\left(\frac{d^2z}{ds^2} - \frac{1}{h_o}\frac{dh_o}{ds}\frac{dz}{ds}\right) \tag{31}$$

$$F_3 = \frac{u_{so}}{ho}\left(F_1 - \frac{G_o}{h_o}\frac{dh_o}{ds}\right)$$

The following three boundary conditions are specified for the solution of Eq. (27):

(a) The entrance-perturbation, circumferential velocity is zero, i.e.,

$$\bar{u}_{\theta 1}\ (0) = 0 \tag{32.a}$$

(b) The entrance loss at the seal entrance is defined by Eq. (15), and the corresponding perturbation-variable relationship is

$$\bar{p}1\ (0) = -\ (1 + \xi)\ \bar{u}s1\ (0) \tag{32.b}$$

(c) The relationship at the exit is provided by Eq. (17) and yields the following perturbation relationship

$$\bar{p}_1\ (1) = C_{de}\ u_{so}\ (1)\ \bar{u}_{s1}\ (1) \tag{32.c}$$

The value for C_{de} depends on the wear-ring seal geometry. Solution of Eq. (27) for the boundary conditions of Eqs. (32) is relatively straightforward, involving successive solutions for displacement and rotation excitations. The complete solution is the sum of the homogeneous solution (which depends on the unknown initial conditions $\bar{p}_1\ (0)$, $\bar{u}_{s1}\ (0)$) and the particular solutions which are proportional to either q_o or α_o. Complete solutions are developed separately for the two vectors on the right-hand side of Eq. (27), which satisfy the boundary conditions of Eqs. (32). By virtue of the problem's linearity, these two solutions may be added to obtain the complete system solution or employed separately to calculate the rotordynamic coefficients. The solution to Eq. (27), due to displacement perturbation, is obtained by setting $\alpha_o = 0$, and may be stated

$$\begin{Bmatrix} \bar{u}_{s1} \\ \bar{u}_{\theta 1} \\ \bar{p}_1 \end{Bmatrix} = \left(\frac{q_o}{\varepsilon}\right) \begin{Bmatrix} f_{1c} + j\ f_{1s} \\ f_{2c} + j\ f_{2s} \\ f_{3c} + j\ f_{3s} \end{Bmatrix} = \left(\frac{q_o}{\varepsilon}\right) \begin{Bmatrix} f_1 \\ f_2 \\ f_3 \end{Bmatrix} \tag{33}$$

The soluton due to angular perturbations is obtained by setting $q_o = 0$ and may be stated

$$\begin{Bmatrix} \bar{u}_{s1} \\ \bar{u}_{01} \\ \bar{p}_1 \end{Bmatrix} = \left(\frac{\alpha_o}{\varepsilon}\right) \begin{Bmatrix} f_{4c} + j\ f_{4s} \\ f_{5c} + j\ f_{5s} \\ f_{6c} + j\ f_{6s} \end{Bmatrix} = \left(\frac{\alpha_o}{\varepsilon}\right) \begin{Bmatrix} f_4 \\ f_5 \\ f_6 \end{Bmatrix} \tag{34}$$

Reaction Forces and Moments

From figure 5, the differential force components acting on a differential-impeller surface area can be stated

$$\begin{aligned} dF_X &= -\ (P\cos\gamma - \tau_{rs}\ \sin\gamma)\ R\ d\theta dS\ \cos\theta + \tau_{r\theta}\ \sin\theta\ R\ d\theta ds \\ dF_Y &= -\ (P\cos\gamma - \tau_{rs}\ \sin\gamma)\ R\ d\theta ds\ \sin\theta - \tau_{r\theta}\ \cos\theta\ R\ d\theta ds \\ dF_Z &= -\ (P\sin\gamma + \tau_{rs}\ \cos\gamma)\ R\ d\theta ds \end{aligned} \tag{35}$$

The shear-stress contribution to these differential-force components has been neglected in prior analysis of seals. The X and Y components are used to define rotordynamic coefficients; the Z component defines the axial thrust. Taking moments of the differential force vector about the origin of the X, Y, Z system yields the following differential moment components.

$$\begin{aligned} dM_X &= \left\{ -[P(R\sin\Upsilon - Z\cos\Upsilon) + \tau_{rs}\,(R\cos\Upsilon + Z\sin\Upsilon)]\,\sin\theta + Z\,\tau_{r\theta}\cos\theta \right\} \\ dM_Y &= \left\{ -[P(R\sin\Upsilon - Z\cos\Upsilon) + \tau_{rs}\,(R\cos\Upsilon + Z\sin\Upsilon)]\,\cos\theta + Z\,\tau_{r\theta}\sin\theta \right\} \\ & \qquad R\; d\theta ds \\ dM_Z &= -\tau_{r\theta}\, R^2\, d\theta ds \end{aligned} \tag{36}$$

The X and Y components yield rotordynamic coefficients; the Z component defines the drag torque.

From Eqs. (35) and (36), the force and moment perturbations are stated

$$F_{X1} = -\varepsilon \int_0^{L_s}\int_0^{2\pi} (P_1\cos\Upsilon - \tau_{rs1}\sin\Upsilon)\cos\theta\, R\, d\theta dS + \varepsilon \int_0^{L_s}\int_0^{2\pi} \tau_{r\theta 1}\sin\theta\, R\, d\theta dS \tag{37a}$$

$$F_{Y1} = -\varepsilon \int_0^{L_s}\int_0^{2\pi} (P_1\cos\Upsilon - \tau_{rs1}\sin\Upsilon)\sin\theta\, R\, d\theta dS - \varepsilon \int_0^{L_s}\int_0^{2\pi} \tau_{r\theta 1}\cos\theta\, R\, d\theta dS \tag{37b}$$

$$M_{X1} = -\varepsilon \int_0^{L_s}\int_0^{2\pi} [P_1(R\sin\Upsilon - Z\cos\Upsilon) + \tau_{rs1}\,(R\cos\Upsilon + Z\sin\Upsilon)]\, R\sin\theta\, d\theta dS + \varepsilon \int_0^{L_s}\int_0^{2\pi} \tau_{r\theta 1}\, ZR\cos\theta\, d\theta dS \tag{37c}$$

$$M_{Y1} = \varepsilon \int_0^{L_s}\int_0^{2\pi} [P_1(R\sin\Upsilon - Z\cos\Upsilon) + \tau_{rs1}\,(R\cos\Upsilon + Z\sin\Upsilon)]\cos\theta\, R\, d\theta dS + \varepsilon \int_0^{L_s}\int_0^{2\pi} \tau_{r\theta 1}\, ZR\sin\theta\, d\theta dS \tag{37d}$$

From Eq. (5), the perturbation shear stresses can be stated

$$\tau_{sr1} = \rho V_i^2 \left(B_{s1}\, u_{s1} + B_{s2}\, u_{\theta 1} + B_{s3}\, h_1\right)$$

$$\tau_{\theta r1} = \rho V_i^2 \left(B_{\theta 1}\, u_{s1} + B_{\theta 2}\, u_{\theta 1} + B_{\theta 3}\, h_1\right) \tag{38}$$

The coefficients of these equations are defined in the appendix. Successive substitutions from (a) Eqs. (9) and (18), (b) Eqs. (19), and (c) Eqs. (21), (24), and (26) into Eqs. (37) yields

$$\frac{F_r + jF_\theta}{F_o} = \frac{(F_{X1} + jF_{Y1})e^{-jf\tau}}{F_o} \tag{39a}$$

$$= -\frac{\varepsilon\pi L_s}{C_d L} \int_o^1 \left\{ \bar{p}_1 \left(\frac{L}{L_s}\right) \frac{dz}{ds} + \bar{u}_{s1} \left[\left(\frac{R}{L_s}\right) \frac{dr}{ds} B_{s1} + j\, B_{\theta 1}\right] + \bar{u}_{\theta 1} \left[\left(\frac{R}{L_s}\right) \frac{dr}{ds} B_{s2} + j\, B_{\theta 2}\right] + \bar{h}_1 \left[\left(\frac{R}{L_s}\right) \frac{dr}{ds} B_{s3} + j\, B_{\theta 3}\right] \right\} r\, ds$$

$$\frac{M_\theta - jM_r}{F_o L} = \frac{(M_{Y1} - jM_{X1})e^{-jf\tau}}{F_o L} \tag{39b}$$

$$= -\frac{\varepsilon\pi L_s}{C_d} \int_o^1 \left\{ \bar{p}_1 \left[\left(\frac{R_i^2}{L L_s}\right) r \frac{dr}{ds} + \left(\frac{L}{L_s}\right) z \frac{dz}{ds}\right] + \bar{u}_{s1} \left[\left(\frac{R_i}{L_s}\right) \left(z \frac{dr}{ds} - r \frac{dz}{ds}\right) B_{s1} + j\, B_{\theta 1}\right] + \bar{u}_{\theta 1} \left[\left(\frac{R_i}{L_s}\right) \left(z \frac{dr}{ds} - r \frac{dz}{ds}\right) B_{s2} + j\, B_{\theta 2}\right] + \bar{h}_1 \left[\left(\frac{R_i}{L_s}\right) \left(z \frac{dr}{ds} - r \frac{dz}{ds}\right) B_{s3} + j\, B_{\theta 3}\right] \right\} r\, ds$$

where

$$F_o = 2R_i L \Delta P \tag{40}$$

Note that

$$\Delta P = P_s - P_e = C_d \frac{\rho V_i^2}{2} \tag{41}$$

is the total pressure drop along the leakage path from impeller discharge to inlet.

Rotordynamic Coefficients for Displacement Perturbations

Eqs. (39) apply for simultaneous displacement and slope perturbations and are solved alternately for displacement and slope perturbations. For the displacement solution, α_o is set equal to zero, and Eqs. (21) and (33) yield

$$f_{rq} = \frac{F_r(f)}{q_o F_o} = -\frac{\pi}{C_d}\left(\frac{L_s}{L}\right)\int_o^1 \left[f_{3c}\left(\frac{L}{L_s}\right)\frac{dz}{ds} + f_{1c}\left(\frac{R_i}{L_s}\right)\frac{dr}{ds} B_{s1} - f_{1s} B_{\theta 1} + f_{2c}\left(\frac{R_i}{L_s}\right)\frac{dr}{ds} B_{s2} - f_{2s} B_{\theta 2} - \left(\frac{LR_i}{L^2_s}\right)\frac{dz}{ds}\frac{dr}{ds} B_{s3}\right] rds$$

$$f_{\theta q} = \frac{F_\theta(f)}{q_o F_o} = -\frac{\pi}{C_d}\left(\frac{L_s}{L}\right)\int_o^1 \left[f_{3s}\left(\frac{L}{L_s}\right)\frac{dz}{ds} + f_{1s}\left(\frac{R_i}{L_s}\right)\frac{dr}{ds} B_{s1} + f_{1c} B_{\theta 1} + f_{2s}\left(\frac{R_i}{L_s}\right)\frac{dr}{ds} B_{s2} + f_{2c} B_{\theta 2} - \left(\frac{L}{L_s}\right)\frac{dz}{ds} B_{\theta 3}\right] rds \quad (42)$$

$$m_{\theta q} = \frac{M_\theta(f)}{q_o F_o L} = \frac{\pi}{C_d}\left(\frac{Ls}{L}\right)\int_o^1 \left[f_{3s} E_1 + f_{1c} E_2 B_{s1} - f_{1s} B_{\theta 1} + f_{2s} E_2 B_{s2} - f_{2s} B_{\theta 2} - \left(\frac{L}{L_s}\right) E_2 \frac{dz}{ds} B_{s3}\right] rds$$

$$m_{rq} = \frac{M_r(f)}{q_o F_o L} = \frac{\pi}{C_d}\left(\frac{Ls}{L}\right)\int_o^1 \left[f_{3c} E_1 + f_{1s} E_2 B_{s1} + f_{1c} B_{\theta 1} + f_{2c} E_2 B_{s2} + f_{2c} B_{02} - \left(\frac{L}{L_s}\right)\frac{dz}{ds} B_{\theta 3}\right] rds$$

where

$$E_1 = \left(\frac{R_i^2}{LL_s}\right) r\frac{dr}{ds} + \left(\frac{L^2}{L_s}\right) z\frac{dz}{ds} \quad (43)$$

$$E_2 = \left(\frac{R_i}{L_s}\right)\left(z\frac{dr}{ds} - r\frac{dz}{ds}\right)$$

The right-hand side of Eqs. (42) is only a function of the frequency-ratio, f, and can be evaluated for selected values of this parameter.

The comparable results from Eq. (1) are

$$
\begin{aligned}
f_{rq}(f) &= \frac{F_r(f)}{q_o F_o} = -(\tilde{K} + f\tilde{c} - f^2\tilde{M}) \\
f_{\theta q}(f) &= \frac{F_\theta(f)}{q_o F_o} = \tilde{k} - f\tilde{C} \\
m_{\theta q}(f) &= \frac{M_\theta(f)}{q_o F_o L} = -(\tilde{K}_{\alpha\varepsilon} + f\tilde{c}_{\alpha\varepsilon} - f^2\tilde{M}_{\alpha\varepsilon}) \\
-m_{rq}(f) &= \frac{M_r(f)}{q_o F_o L} = \tilde{K}_{\alpha\varepsilon} - f\tilde{C}_{\alpha\varepsilon} - f^2 m_{\alpha\varepsilon}
\end{aligned}
\tag{44}
$$

Where the nondimensional coefficients are defined by

$$
\begin{aligned}
&\tilde{K} = KC_i/F_o,\ \tilde{k} = kC_i/F_o,\ \tilde{M} = MC_i\,\omega^2/F_o \\
&\tilde{C} = CC_i\omega/F_o,\ \tilde{c} = cC_i\omega/F_o \\
&\tilde{K}_{\alpha\varepsilon} = K_{\alpha\varepsilon}C_i/LF_o,\ \tilde{C}_{\alpha\varepsilon} = C_{\alpha\varepsilon}\,C_i\omega/LF_o,\ \tilde{M}_{\alpha\varepsilon} = M_{\alpha\varepsilon}C_i\omega^2/LF_o \\
&\tilde{k}_{\alpha\varepsilon} = k_{\alpha\varepsilon}C_i/LF_o,\ \tilde{c}_{\alpha\varepsilon} = c_{\alpha\varepsilon}C_i\omega/LF_o\ ,\ m_{\alpha\varepsilon}C_i\omega^2/LF_o
\end{aligned}
\tag{45}
$$

The dynamic coefficients are obtained by equating the right-hand sides of Eqs. (42) and (44) and by carrying out a least-square curve fit on the results from Eq. (42).

Rotordynamic Coefficients for Slope Perturbations

Applying the procedure of the preceding section to Eqs. (42) with $q_o = 0$ yields

$$
\begin{aligned}
f_r(f) = \frac{F_r(f)}{\alpha_o F_o} = -\frac{\pi}{C_d}\left(\frac{L}{Ls}\right)\int_o^1 \Big[& f_{6c}\left(\frac{L}{Ls}\right)\frac{dz}{ds} + f_{4c}\left(\frac{Ri}{Ls}\right)\frac{dr}{ds}B_{s1} - f_{4s}B_{\theta 1} \\
& + f_{5c}\left(\frac{Ri}{Ls}\right)\frac{dr}{ds}B_{s2} - f_{5s}B_{\theta 2} - G_o\left(\frac{Ri}{Ls}\right)\frac{dr}{ds}B_{s3}\Big]\,rds
\end{aligned}
$$

$$
f_\theta(f) = \frac{F_\theta(f)}{\alpha_o F_o} = -\frac{\pi}{C_d}\left(\frac{L}{Ls}\right)\int_o^1 \Big[f_{6s}\left(\frac{L}{Ls}\right)\frac{dz}{ds} + f_{4s}\left(\frac{Ri}{Ls}\right)\frac{dr}{ds}B_{s1} + f_{4c}B_{\theta 1}
$$

$$+ f_{5s}\left(\frac{Ri}{Ls}\right) B_{s2} + f_{5c} B_{\theta 2} - G_o B_{\theta 3}\Big] rds \tag{46}$$

$$m_{\theta\alpha}(f) = \frac{M_\theta(f)}{\alpha_o F_o L} = -\frac{\pi}{C_d}\left(\frac{L}{Ls}\right)\int_o^1 \Big[f_{6c} E_1 + f_{4c} E_2 B_{s1} - f_{4s} B_{\theta 1}$$

$$+ f_{5c} E_2 B_{s2} - f_{5c} B_{\theta 2} - G_o E_2 B_{s3}\Big] rds$$

$$m_{r\alpha}(f) = \frac{M_r(f)}{\alpha_o F_o L} = -\frac{\pi}{C_d}\left(\frac{L}{Ls}\right)\int_o^1 \Big[f_{6s} E_1 + f_{4s} E_2 B_{s1} + f_{4c} B_{\theta 1}$$

$$+ f_{5s} E_2 B_{s2} + f_{5c} B_{\theta 2} - G_o B_{\theta 3}\Big] rds$$

Eq. (1) yields the corresponding solution format

$$f_{r\alpha}(f) = \frac{F_r(f)}{\alpha_o F_o} = -(\tilde{K}_{\varepsilon\alpha} + f\,\tilde{c}_{\varepsilon\alpha} - f^2\tilde{M}_\alpha) \tag{47}$$

$$f_{\theta\alpha}(f) = \frac{F_\theta(f)}{\alpha_o F_o} = (\tilde{k}_{\varepsilon\alpha} - f\tilde{C}_{\varepsilon\alpha} - \tilde{f}^2 m_{\varepsilon\alpha})$$

$$m_{\theta\alpha}(f) = \frac{M_\theta(f)}{\alpha_o F_o L} = (\tilde{k}_\alpha + fc_\alpha - f^2 M_\alpha)$$

$$-m_{r\alpha}(f) = -\frac{M_r(f)}{\alpha_o F_o L} = \tilde{k}_\alpha - \tilde{f}C_\alpha - \tilde{f}^2 m_\alpha$$

where

$$\begin{aligned}
&\tilde{K}_{\varepsilon\alpha} = K_{\varepsilon\alpha}/F_o,\ \tilde{k}_{\varepsilon\alpha} = k_{\varepsilon\alpha}/F_o,\ \tilde{M}_{\varepsilon\alpha} = M_{\varepsilon\alpha}\omega^2/F_o \\
&\tilde{C}_{\varepsilon\alpha} = C_{\varepsilon\alpha}\omega/F_o,\ \tilde{c}_{\varepsilon\alpha} = c_{\varepsilon\alpha}\omega/F_o,\ \tilde{m}_{\varepsilon\alpha} = m_{\varepsilon\alpha}\omega^2/F_o \\
&\tilde{K}_\alpha = K_\alpha/F_o L,\ \tilde{k}_\alpha = \tilde{k}_\alpha/F_o L,\ \tilde{M}_\alpha = M_\alpha\omega^2/F_o L \\
&\tilde{C}_\alpha = C_\alpha\omega/F_o L,\ \tilde{c}_\alpha = c_\alpha\omega/F_o L,\ \tilde{m}_\alpha = m_\alpha\omega^2/F_o L
\end{aligned} \tag{48}$$

The rotordynamic coefficients are obtained by equating the right-hand side of Eqs. (46) and (47).

Predictions and Comparison to Experimental Results

Figures 6(a) and 6(b) illustrate, respectively, a nominal pump-impeller geometry with a conventional wear-ring seal and a modified pump impeller with a face seal. Bolleter et al. tested the face-seal impeller to eliminate the forces which would normally be generated by the wear-ring seal. Their tests were at best efficiency point (BEP)

with the pump running at 2000 rpm, while developing 68m of head and 130 l/sec of flow rate. The impeller has seven blades and an impeller exit angle of 22.5°. The test fluid is water at 80°F.

The present analysis requires an estimate of the ΔP across the impeller versus the total head rise of the stage. At U. Bolleter's suggestion, the impeller ΔP was estimated to be 70% of the total ΔP of the pump. An estimate of the inlet tangential velocity is also required. Fortunately, pitot-tube measurements are available, indicating that the inlet tangential velocity is approximately 50% of the exit impeller surface velocity; i.e., $u_{\theta o}(o) \simeq 0.5$. This is in contrast to a theoretically-predicted tangential velocity of $0.72\, R_i\omega$ based on the blade-exit angle. Adkins' measurements at Cal Tech [12] also show substantially lower exit tangential velocities than predicted from exit blade angles.

Both walls of the impeller were assumed to be smooth and represented by Yamada's [13] test data; mr = ms = -0.25, nr = ns = 0.079. The inlet loss for the impeller, ξ, was assumed to be 0.1. The discharge coefficient for the seal was calculated iteratively as follows. With an assumed C_{de}, Eqs. (14), (15), and (17) were used to calculate the leakage through the impeller annulus and the pressure and tangential-velocity upstream of the seal. The seal is then analyzed (with the same equations) using the calculated seal inlet pressure and tangential velocity to determine leakage and C_{de}. The iteration continues until the leakage predictions for the exit seal and the impeller annulus agree.

Figures 7(a) and (b) illustrate the predicted radial and tangential force coefficients f_{rq} and $f_{\theta q}$ versus the whirl frequency ratio $f = \Omega/\omega$ for the face-seal, impeller. Results are presented for $u_{\theta o}(0) = 0.5$, 0.6, and 0.7. The $u_{\theta o}(0) = 0.5$ data of these figures is generally consistent with expectations based on experience with seals except for a slight "dip" in f_{rq} and "bump" in $f_{\theta q}$. However, the peaks exhibited at higher value for $u_{\theta o}$ are quite unexpected. They arise primarily due to the centrifugal acceleration term in the path-momentum equation. If the term

$$\frac{2u_{\theta o}}{R}\,\frac{dr}{ds} \Big/ b^2,$$

is dropped from the A_{2s} definition of Appendix A, the "peaks" are substantially eliminated from the force predictions.

Figure 8(a) and (b) provide predictions for f_{rq} and $f_{\theta q}$ for the conventional wear-ring-seal impeller of figure 6(a). The predicitons are only for the impeller and do not include the exit wear-ring seal. The $f_{\theta q}$ results for the two impellers are quite similar; however, the f_{rq} values are generally larger for the face-seal impeller.

Table 1 below provides zeroth-order-solution results for the conventional-seal impeller of figure 6(b).

Observe that the leakage is reduced by increasing $u_{\theta o}(0)$. Also observe the relatively high seal-inlet-tangential velocity prediction for the exit seals, which will predictably lead to increased cross-coupled stiffness coefficients and decreased rotor stability. The Reynolds number values suggest that care should be taken in extrapolating impeller force data from one operating condition to another. Specifically, changes in temperature or operating media would be expected to yield significant changes in force data.

The freqency-dependency of f_{rq} and $f_{\theta q}$ exhibited in figures 7 and 8 for $u_{\theta o}(0) = 0.6, 0.7$ can not be modeled by the rotordynamic-coefficient model on Eq. (1). Stated differently, The quadratic dependency of f_{rq} and $f_{\theta q}$ on f, which is specified in Eq. (44), is simply not true. A significantly more complicated dependency is clearly in order. While these results of figures 7 and 8 are surprising, recent data from the Cal Tech program by Franz and Arndt [14] are qualitatively similar.

The $u_{\theta o}(0) = 0.5$ results of figure 7 are reasonably modeled by a quadratic dependency of f and can be modeled by rotordynamic coefficients. A comparison of predicted and measured coefficients is provided in Table 2.
Keeping in mind that the present theory does not account for the momentum flux exiting from the impeller or the pressure forces on the impeller exit, the comparison between theory and experiment of Table 1 is encouraging. The prediction of C and M are good. The results for k are consistent with Adkins [12] statement that the impeller annulus accounts for approximately one half of the measured stiffness values in Cal Tech test results. The results for K and c are obviously dissappointing; perhaps these coefficients depend more heavily on the impeller-diffuser interaction forces.

Conclusions and Extensions

An analysis has been developed for the forces on the shroud of an impeller. The "bulk-flow" nature of the analysis restricts its applicability to impellers having fairly small clearances between the impeller shroud and casing.

The results of the analysis are unexpected in that resonances of the fluid system are predicted at inlet tangential velocities which are higher than approximately $0.5\ R_i\omega$. Conventional rotordynamic-coefficient models are not an adequate representation of rotor forces if the resonances are present. The resonance phenomenon predicted by this analysis are in qualitative agreement with recent measurements from Cal Tech [14].

Rotordynamic-coefficients predictions from this analysis are in reasonable agreement with test results from Bolleter et al. [7], for the direct damping and cross-coupled stiffness coefficients, C and k.

The analysis which was developed in this paper for impeller shrouds can also be applied to seals and provides an expanded

capability with respect to clearances as a function of axial or path coordinate. Prior analyses have been developed for either constant-clearance or convergent-tapered seals. The present analysis would apply for any continuously varying clearance function. This option can be directly used to account for elastic deformation of the seal bore due to pressure or other loading. It also provides possibilities for optimizing the clearance function to maximize stiffness, damping, etc.

The addition of shear-stress contributions in the present analysis made very little difference in seal calculations. As yet, no comparisons have been made on impeller force calculations with and without the shear-stress contributions.

The importance of the moment coefficients, which are defined by the represent analysis, are as yet undetermined. Current rotordynamic codes are not yet up to accept these coefficients; however, a code is under development at TAMU which will account for these coefficients and can be used to determine their importance.

The significance of the "resonance" phenomenon, which is predicted by the present analysis, on rotordynamics also remains unsettled. An analysis of the phenomenon is planned which will include curvefitting the $f_{rq}(f)$ and $f_{\theta q}(f)$ predictions and examining their influence on a Jeffcott rotor model.

The present analysis can be readily extended to account for axial force coefficients. An extension of this nature is projected for the coming year.

APPENDIX A

Perturbation Coefficients

$$A_{1s} = [\sigma_s(1-ms) + \sigma_r (1-mr)]\, u_{so}^2/2h_o$$

$$A_{2s} = -\frac{2u_{\theta o}}{r}\frac{dr}{ds}/b^2 + [\sigma_r (mr+1)\, \beta_o + \sigma_s (ms+1)\, \beta_1]\, u_{so}/2$$

$$A_{3s} = \frac{du_{so}}{ds} + [(2 + mr)\, \sigma_r + (2 + ms)\, \sigma_s]\, u_{so}/2$$

$$-[(1+mr)\, \sigma_r\, \beta_o\, (u_{\theta o}-r) + (1+ms)\, \sigma_s\, \beta_1\, u_{\theta o}]\, /2$$

$$2A_{1\theta} = u_{so}\, [(1-mr)\, (u_{\theta o}-r)\, \sigma_r + (1-ms)\, u_{\theta o}\, \sigma_s + 2\frac{u_{\theta o}}{r}\frac{dr}{ds}]/ho$$

$$2A_{2\theta} = u_{so}\, (\sigma_r+\sigma_s) + \sigma_r\, (mr+1)\, (u_{\theta o}-r)\, \beta_o + 2\frac{u_{so}}{r}\frac{dr}{ds}$$

$$+ \sigma_s\, (ms+1)\, u_{\theta o}\, \beta_1$$

$$2A_{3\theta} = \sigma_r (u_{\theta o}-r) [mr - (1+mr) \beta o (u_{\theta o}-r)/u_{so}]$$
$$+ \sigma_s u_{\theta o} [ms - (1+ms) \beta 1 u_{\theta o}/u_{so}]$$

$$\beta_o = (u_{\theta o}-r)/b^2 u_{so} \{1 + [(u_{\theta o}-r)/bu_{so}]^2\}$$

$$\beta_1 = u_{\theta o}/b^2 u_{so} [1 + (u_{\theta o}/bu_{so})^2]$$

$\tau_{r\theta}$ Perturbation Coefficients

$$B_{\theta 1} = \lambda_r (1+mr)(u_{\theta o}-r)[1-\beta_o(u_{\theta o}-r)/u_{so}]/2b$$

$$B_{\theta 2} = \lambda_r [u_{so}+(1+mr)(u_{\theta o}-r)\beta o]/2b$$

$$B_{\theta 3} = \lambda_r mr (u_{\theta o}-r)u_{so}/2bh_o$$

τ_{rs} Perturbation Coefficients

$$B_{s1} = \lambda_r[(2+mr) u_{so} - (1+mr) \beta_o (u_{\theta o} -r)]/2$$

$$B_{s2} = \lambda_r(1+mr) \beta_o u_{so}/2$$

$$B_{s3} = \lambda_r m_r u_{so}^2/2h_o$$

REFERENCES

1. Lomakin, A., "Calculation of Critical Speed and Securing of the Dynamic Stability of the Rotor Hydraulic High Pressure Machines with Reference to Forces Arising in Seal Gaps," Energomashinostroenie, Vol. 4, 1958.

2. Childs, D., and Kim, C-H., "Test Results for Round-Hole-Pattern Damper Seals: Optimum Configurations and Dimensions for Maximum Net Damping," 85-Trib-16, ASME-ASLE Joint Lubrication Conference, Atlanta, GA, 8-10 October, 1985; also recommended for ASME Trans., Jl. of Tribology Technology.

3. Childs, D., and Kim, C-H., "Analysis and Testing for Rotordynamic Coefficients of Turbulent Annular Seals with Different Directionally Homogeneous Surface Roughness Treatment for Rotor and Stator Elements," ASME Trans. Journal of Tribology Technology, Vol. 107, July 1985, pp. 296-306.

4. von Pragenau, G. L., "Damping Seals for Turbomachinery," NASA Technical Paper 1987, 1982.

5. Jery, B., Acosta, A. J., Brennen, C. E., Caughey, T. K., "Hydrodynamic Impeller Stiffness, Damping and Inertia in the Rotordynamics of Centrifugal Pumps," Proceedings of Workshop on Rotordynamics Instability Problems in High Performance Turbomachinery, Texas A&M University, College Station, TX, NASA Conference Publication 2338, May 1984, pp. 137-160.

6. Ohashi, H., and Shoji, H., "Lateral Fluid Forces Acting on a Whirling Centrifugal Impeller in Vaneless and Vaned Diffuser," Proceedings of Workshop on Rotordynamics Instability Problems in High Performance Turbomachinery, Texas A&M University, College Station, Texas, NASA Conference Publication 2338, May 1984, pp. 109-122.

7. Bolleter, U., Wyss, A., Welte, I., and R. Sturchler, "Measurement of Hydrodynamic Matrices of Boiler Feed Pump Impellers," ASME Paper 85-DET-147, 10th Biennial Conference on Mechanical Vibration and Noise, Cincinnati, Ohio, 10-13 September 1985.

8. Massey, I. C.,, "Subsynchronous Vibration Problem in High Speed Multistage Centrifical Pumps," Proceedings of the 14th Turbomachinery Symposium, Turbomachinery Laboratories, Mechanical Engineering Dept., Texas A&M University, College Station, Texas, October 22-24, 1985, pp. 11-16.

9. Childs, D., and Moyer, D., "Vibration Characteristics of the HPOTP (High Pressure Oxygen Turbopump) of the SSME (Space Shuttle Main Engine)." ASME Trans. J. of Engineering for Gas Turbine, and Power, Vol. 107, January 1985, pp. 152-159.

10. Childs, D. W., "Rotordynamic Moment Coefficients for Finite-Length Turbulent Seals," Proceedings IFTOMM Conference on Rotordynamic Problems in Power Plants, 28 September - 1 October 1981.

11. Hirs, G. G., "A Bulk-Flow Theory for Turbulence in Lubricant Film," ASME Journal of Lubrication Technology, April 1973, pp. 137-146.

12. Adains, D. R., "Analyses of Hydrodynamic Forces on Centrifugal Pump Impellers," Report Number 200.23, California Institute of Technology, 1985.

13. Yamada, Y., "Resistance of Flow Through Annulus with an Inner Rotating Cylinder," Bul. JSME, 1962, Vol. 5., No. 18, pp. 301-310.

14. Franz, R. and Arndt, N., "Measurement of Hydrodynamic Forces on the Impeller of HPOTP of the SSME, Report Number E249.2, California Institute of Technology, March 1986.

$U_{\theta o}(0)/R_i\ \omega$	0.5	0.6	0.7
$U_{\theta o}(1)/R(1)\omega$	0.884	0.947	0.996
$\dot{m}$(Kg/sec)	4.03	3.75	3.44
$R_{ao} = 2V_iC_i/\nu$	73,300	68,100	62,600

Table 1. Zeroth-order-solution results for the conventional-wear-ring impeller.

	Measured	Theory Face-Seal Impeller
K(N/m)	-.5×106	$-.042\times10^6$
k(N/m)	.6×106	$.288\times10^6$
C(N sec/m)	2570*	2020
c(N sec/m)	7610	2290
M (kg)	29.6	8.96
m (kg)	10.8	-0.009

*Combined viscous and hysteretic damping.

Table 2. Theory versus experiment for the face-seal impeller.

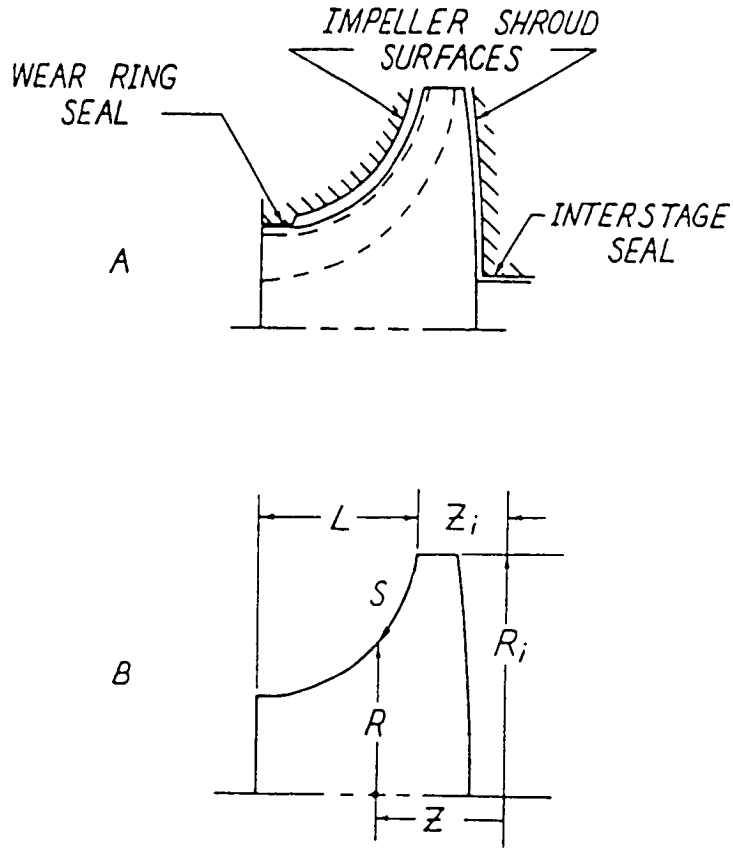

Figure 1. Impeller stage.

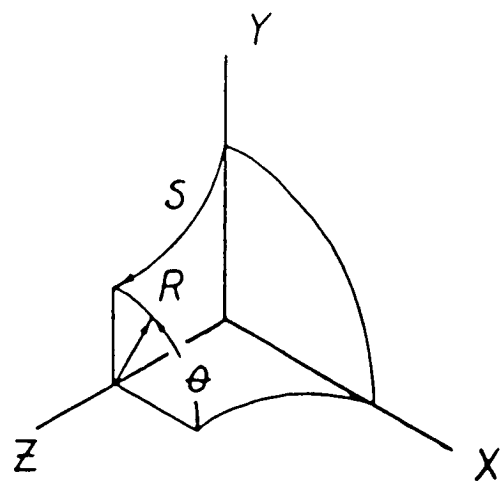

Figure 2. Impeller surface geometry.

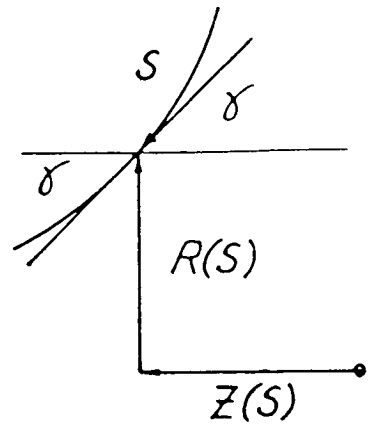

Figure 3. Local attitude angle of impeller surface.

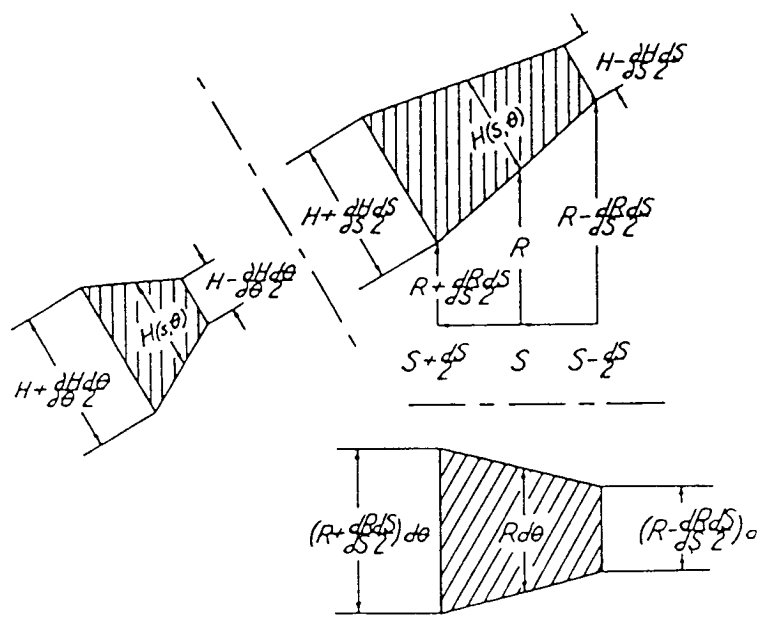

Figure 4. Differential-fluid element.

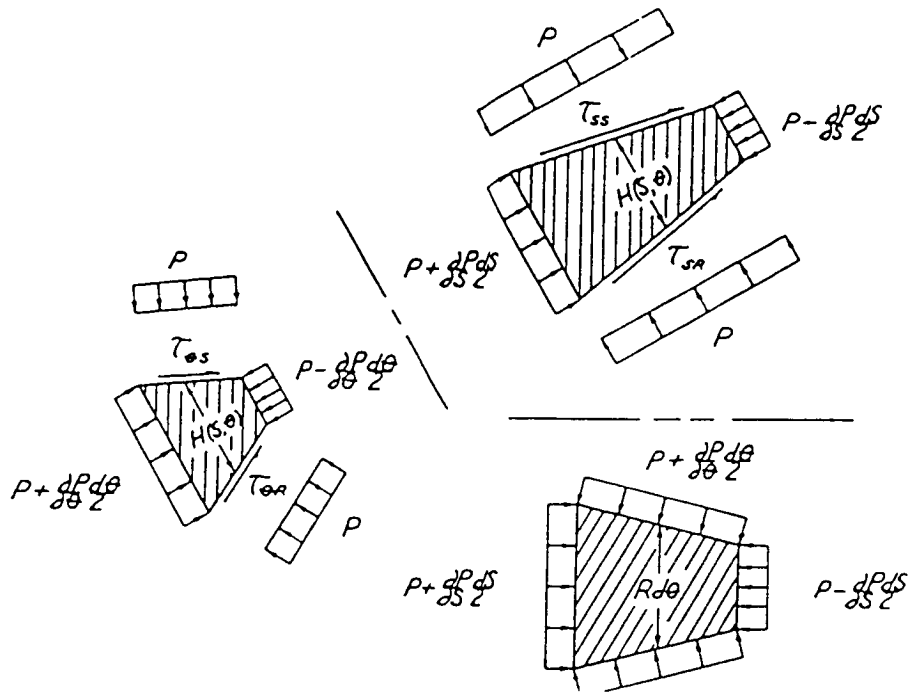

Figure 5. Free-body diagram for differential-fluid element.

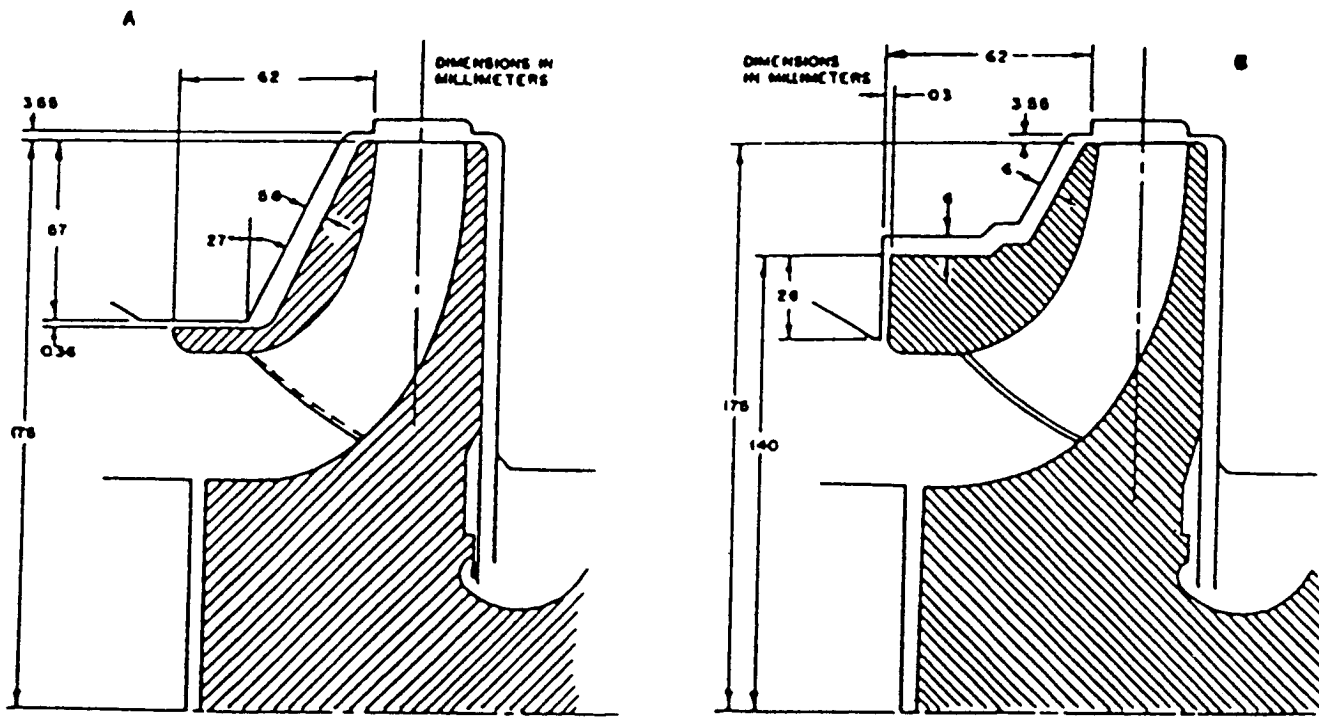

Figure 6. Nominal configuration of Sulzer test impeller [7] with conventional wear-ring seal.

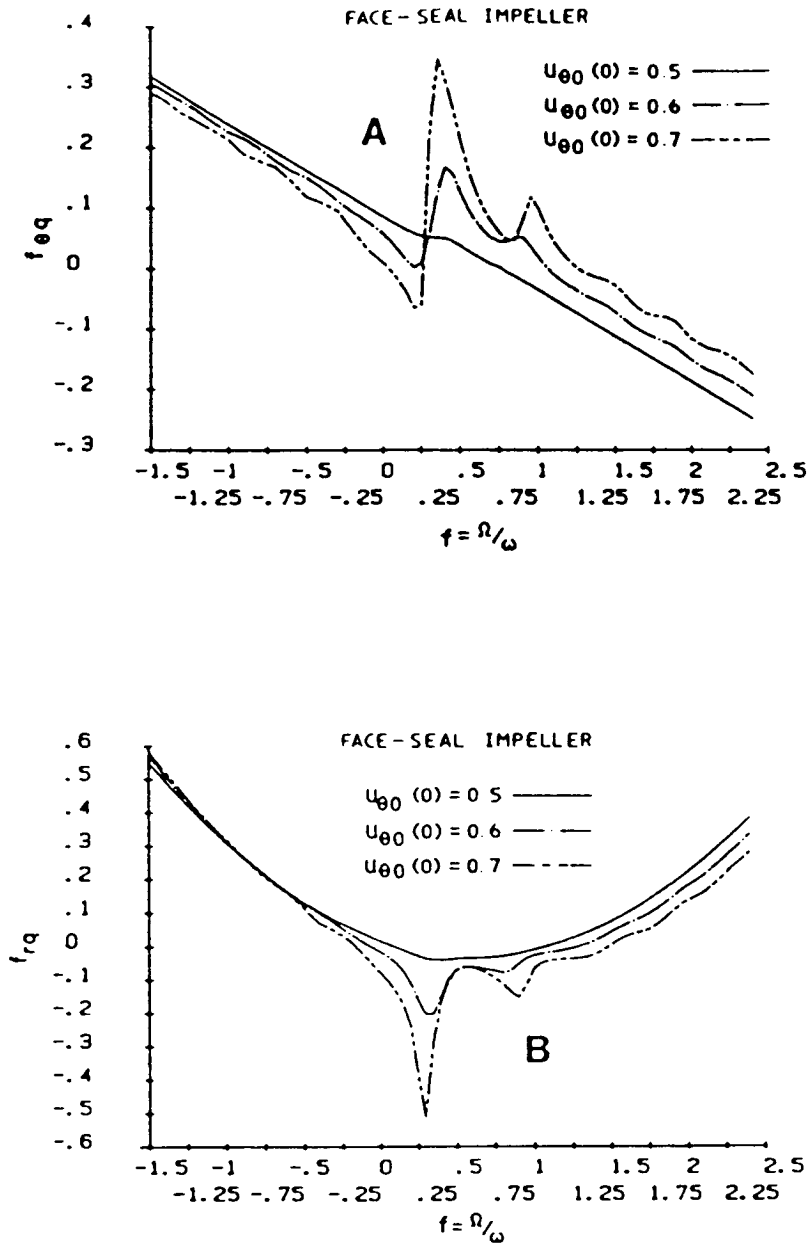

Figure 7. Nondimensional force coefficients for the face-seal impeller; A tangential-force coefficient, B radial-force coefficient.

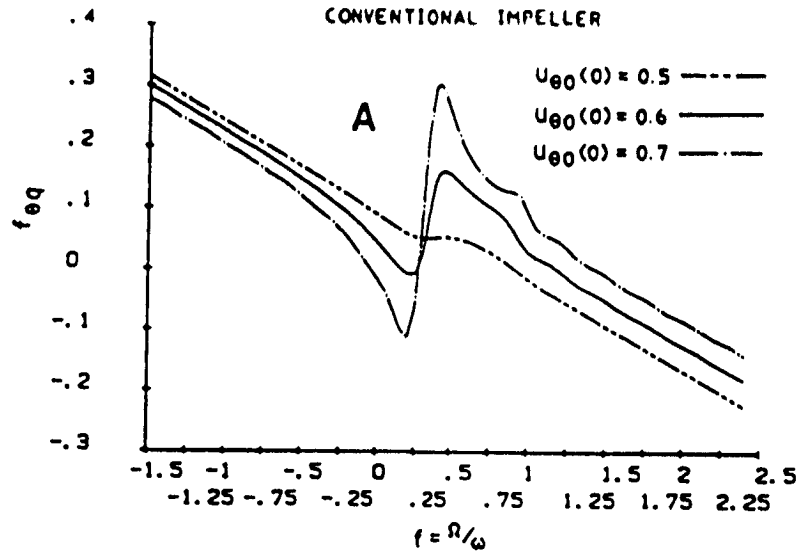

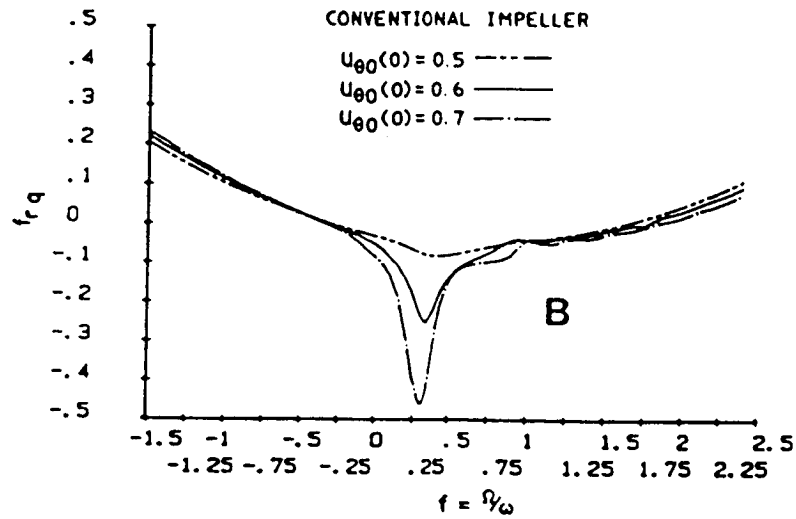

Figure 8. Nondimensional force coefficients for the conventional impeller; A tangential-force coefficient, B radial-force coefficient.